International Journal of Automotive Technology, Vol. 8, No. 5, pp. 605–614 (2007)

1229-9138/2007/036-09

NOISE REFINEMENT OF A VEHICLE BY REDUCTION OF THE AXLE GEAR WHINE NOISE BASED ON STRUCTURAL MODIFICATION USING FEM AND BEM

S. J. KIM, J. Y. LEE and S. K. LEE*

Acoustics and Dynamics, Department of Mechanical Engineering, Inha University, Incheon 402-751, Korea

(Received 12 March 2007; Revised 16 August 2007)

ABSTRACT–This paper presents the research results for the reduction of a gear whine noise based on experimental and analytic methods. The test vehicle has a whine noise problem at the passenger seats in a sport utility vehicle. To identify the transfer path of the interior noise due to the axle system, a vibration path analysis, modal analysis and operational deflection shape analysis are systematically employed. By using these various methods, it has been found that the interior noise generated by the axle system was airborne noise. To reduce and predict the whine generated by the axle system, structural modifications for the axle system are performed by using FEM and BEM techniques. The structural modification of the axle cover is suggested for the reduction of whine noise.

KEY WORDS : Axle noise, Whine noise, EMA, FEM, BEM, SUV, Airborne noise

1. INTRODUCTION

As NVH (Noise Vibration Harshness) technology has advanced, the overall level of interior noise, which is mainly due to a major component, such as the engine, tires, body structure, road and wind, is reduced dramatically (Lee *et al.*, 2005; Donley *et al.*, 1992; Sun *et al.*, 2003). However, the whine noise (Becker and Yu, 1999a), which masks these major noise sources, becomes the important noise source and worsens a car's sound quality. In particular, the whine noise due to the axle system of a sporty utility vehicle (SUV) becomes one of the dominant noise sources (Becker and Yu, 1999b; Kim and Lee, 2007). In this study, various methods were systematically employed in order to reduce the whine noise of the axle system of a sport utility vehicle. First, the interior noise of the test vehicle was measured. The mode shape and the operational deflection shape of the axle system were obtained experimentally in order to identify the source of the whine noise (Wyckaert *et al.*, 1995). Secondly, the structure of the axle system was optimized to reduce the whine noise by using FEM (finite element method) (Paras, 2003; Blakely, 1991; Walter and Kaiser, 1990) and BEM (boundary element method). The FE model of the axle system is confirmed by comparing the result of analytic modal analysis with that of experimental modal analysis. The BEM is also used for predicting the whine noise radiating from the axle system. The boundary condition of the axles system is obtained throughout the forced vibration analysis of the axle system. For force vibration analysis of the axle system, the bearing force of the axle system is inversely calculated by using the inverse force identification method (Warwick and Van der Auweraer, 1993). The method used for the inverse problem is singular value decomposition.

*Corresponding author. e-mail: sangkwon@inha.ac.kr

2. BASE LINE TEST

2.1. Measurement of Interior Noise

The test vehicle is an SUV car with 5-step gear ratio. The number of teeth of the pinion gear of the test axle system is 9, and the number of ring gear teeth is 44. Therefore, the gear ratio of the axle system is 4.89. The engine loaded on the test SUV is a 5-cylinder diesel engine. The vehicle being tested for noise and vibration is driven from 40 km/h to 130 km/h, since the whine noise occurs around this speed. The speed of the input propeller shaft of the axle system at 40 km/h is 1400 rpm and 4400 rpm at 130 km/h. As a baseline test, the interior noise at the front seat and the rear seat of the test vehicle was measured to evaluate the whine noise due to the axle system. The results of interior noise are shown in Figure 1 and Figure 2. Figure 1 shows the Colormap analysis for interior noise measured at the rear seat of the test vehicle. Figure 2 shows the order analysis from the same data.

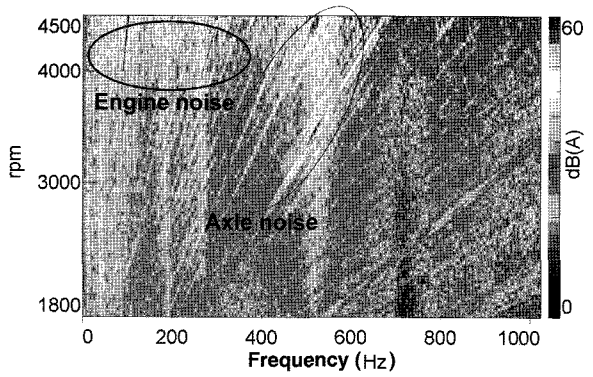

Figure 1. Colormap analysis for the interior noise.

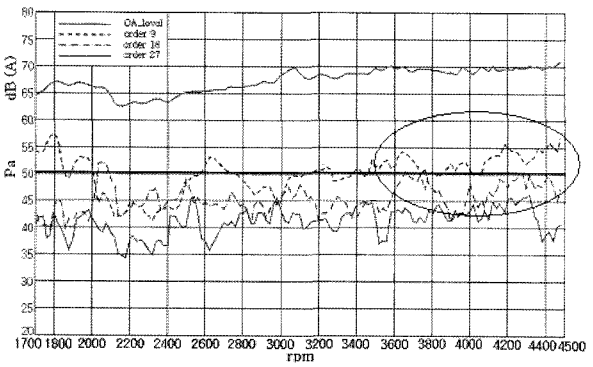

Figure 2. Order analysis for the interior noise.

The high-pressure level at the low frequency region, as shown in Figure 1 is caused by the diesel engine. In this region, the low order components of the rotating speed of the crankshaft of the engine are induced by the combustion of the diesel engine with 5 cycles. These low order components are the major contributors to the increase of the overall level of interior noise of the test vehicle. In Figure 2, the overall sound pressure level of interior noise is 65~70dBA. The sound pressure level of the 9th order, which is not only 9 times the rotation speed of the propeller shaft but also the fundamental meshing frequency due to the meshing between the tooth of pinion gear and the tooth of ring gear in the axle system, is 5~20dBA less than the overall sound pressure level. The sound pressure level of the 18th order, which is the 2nd harmonic of the fundamental meshing frequency and that of the 27th order, which is the 3rd harmonic, is 20~30dBA less than the overall level, respectively. Therefore, the major whine noise associated with the axle system is the sound pressure of the 9th order since the whine noise in an axle system is caused by the tooth meshing. The sound pressure level of the 9th order at 3600 rpm, 4200 rpm and 4400 rpm is over 50dBA, which is the maximum target level of the whine noise due to the axle system in this project.

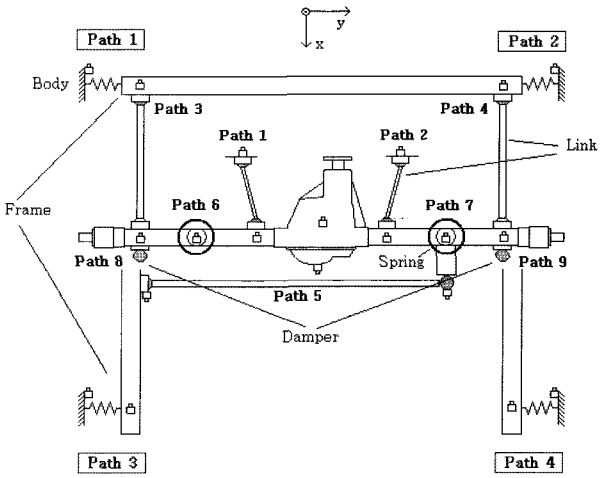

Figure 3. Bottom view of the test vehicle and Illustration of the 5-link suspension system, the axle system and the chassis frame.

During acceleration of the test vehicle, the whine noise correlated with the axle noise is recognized in the region between 80 km/h and 120 km/h (3000~4200 rpm). From the point of view sound quality, the whine noise at high frequency is louder than that at low frequency (Zwicker and Fastl, 1999; Lee and Chae, 2004; Leè *et al.*, 2005). Therefore, the aim of this study was to reduce the sound pressure level of the 9th order to 3dBA from 55dBA to 52dBA.

2.2. Identifying Vibration Transmission Path

The axle system of the test vehicle is linked to a 5-link suspension, which is connected to the chassis frame. The chassis frame is mounted on the car body. Figure 3 shows the bottom view of the test vehicle and illustrates the 5-link suspension system, the axle system, and the chassis frame. The axle system consists of the carrier, carrier cover, axle shaft, shaft bearing, and axle shaft housing. The vibration of the axle system is transferred to the car body through the 5-link system and the chassis frame as shown in Figure 3.

In this 5-link suspension system, there are nine vibration transfer paths from the axle system to the chassis frame. Paths 1 and 2 are the vibration transfer paths from the axle system to the chassis frame through short links L1 and L2. Paths 3, 6 and 8 are the vibration transfer paths from the left side of the axle system to the chassis frame through long links L3. Paths 4, 7 and 9 are the vibration transfer paths from the right side of the axle system to the chassis frame through long links L4. Path 5 is the cross vibration transfer path from the right side of the axle system to the left side of the chassis frame through cross-link L5. Along these paths, there are isolation rubbers not only between the axle system and link but also between

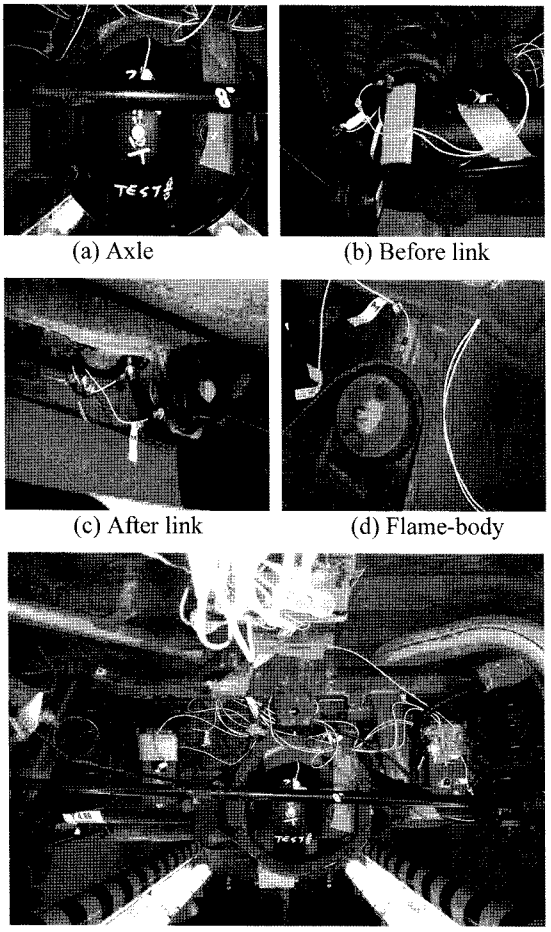

(a) Axle (b) Before link

(c) After link (d) Flame-body

(e) Botton view of the axle system in SUV car

Figure 4. Photo illustrations of the axle system and accelerometer used in the test.

the link and chassis frame. Finally, there is again a mount rubber between the chassis frame and the car body. We measured the acceleration before and after the isolation rubber and mount rubber to see the effect of isolation. The rubber has a damping property, which exchanges the vibration energy with heat energy. The vibrations at several parts of the axle system were also measured by using accelerometers attached on the axle system as shown in Figure 4 to identify the transfer path of the vibration from the axle system to the car body. Figure 5 shows the waterfall analysis for vibration data measured at the accelerometer attached on the cover of the axle carrier. According to the results, there are two major resonances. One resonance occurs at 3600~4200 rpm (540 Hz~630 Hz) due to the 9th order component, and the other resonance occurs at 3600~4400 rpm (1080 ~1290 Hz) due to the 18th order component. Comparing the results for vibration data measured on the axle system (as shown in Figure 5) with the results for the interior noise (as shown in Figure 2), it is inferred that the interior

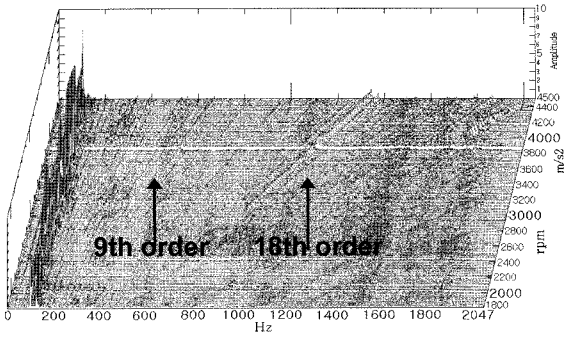

Figure 5. Waterfall analyses for vibration data measured at the accelerometer attached on the cover of axle carrier.

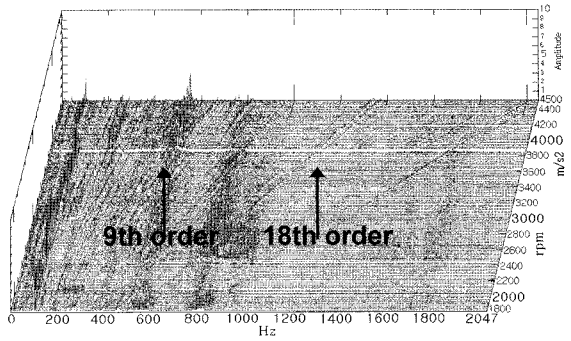

Figure 6. Waterfall analysis for the vibration data measured at the axle system before link L4.

noise due to 9th order around 3600 rpm~4000 rpm is correlated to the 9th order vibration of the axle system. The interior noise due to 18th order is not considered in this paper since its sound pressure level is less than 50dBA. However, the vibration of the axle system affects the interior noise of the test vehicle.

This vibration of the axle system affects the interior noise via two different paths. One is the airborne noise and the other one is the structure-borne noise. In order to identify whether the correlation between the interior noise and the vibration of the axle system is structure-borne or airborne, the vibration measured along the transfer paths was analyzed. The vibration of the axle carrier in the axle system, as shown in Figure 5, is transferred to the link throughout the axle shaft housing. Figure 6 shows the waterfall analysis of vibration data measured on the axle shaft housing. From these results, we find that the 9th order component is still at a high level. However, the vibration of the axle system is reduced through the isolation rubber of the links and the mounting rubber of the chassis frame mounts. Figure 7 shows the waterfall analysis for the vibration data measured at the bracket before and after the isolation rubber of link L4. In the waterfall analysis for vibration data measured at the link system as shown in Figure 7,

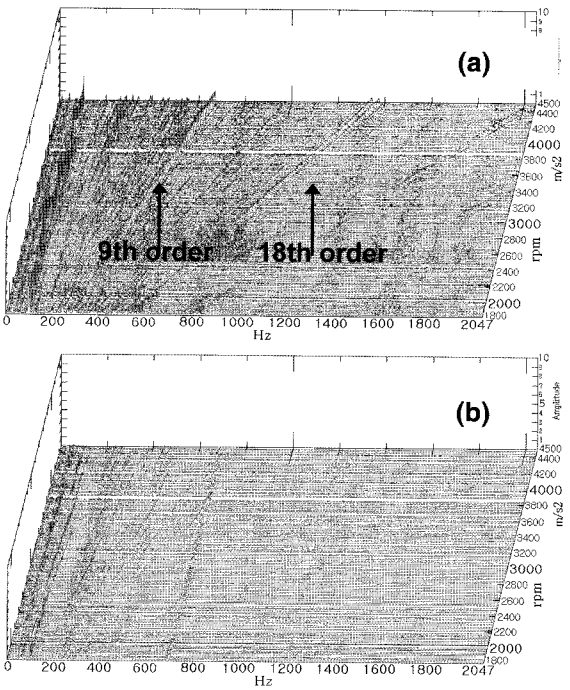

Figure 7. Waterfall analyses for the vibration data measured at the bracket before and after isolation rubber of link L4 (a) before isolation rubber of link L4 (b) after isolation rubber of link L4.

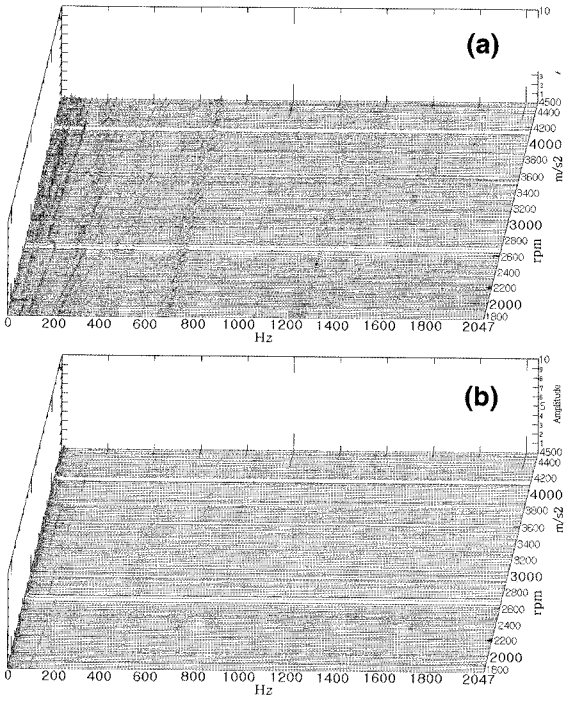

Figure 8. Waterfall analyses for the vibration data measured at the bracket before and after isolation rubber of link L2 (a) before mounting rubber of the path 2. (b) after mounting rubber of the path 2.

the vibration level is reduced by 20dB throughout the isolation rubber of link L4. This vibration is reduced enough throughout the mounting rubber of the chassis frame. Figure 8 shows the waterfall analysis for the vibration data measured at the bracket before and after the mounting rubber of the right chassis frame of path 2. Finally, the vibration of the axle system is completely reduced by passing the mount rubber of the chassis frame as shown in Figure 8; the 9th order component vibration of the axle system (as shown in Figure 5 and Figure 6) is transferred from the axle system to the car body. All other vibration transfer paths also have similar results and do not affect the interior noise. Therefore, it is concluded that the interior noise of the 9th order component is not associated with structure-borne noise but is correlated with the vibration of the axle system.

This vibration of the axle system disturbs the air around the axle system and radiates the noise. This radiated noise is the airborne noise, which is directly transferred into the inside of the car from the axle system. The effect of structure-borne noise due to the vibration transmission is not considerable in this project. To reduce this airborne noise, structural modification of the axle system is required and should be optimized.

3. EXPERIMENTAL MODAL ANALYSIS (EMA) AND OPERATIONAL DEFLECTION SHAPE (ODS)

In the previous section, it was known that the 9th order component of the interior noise is due to airborne noise and it is correlated directly with the noise radiated by vibration of the axle structure at a frequency around 540~630 Hz. In order to obtain the mode shape of the axle structure at this frequency, experimental modal analysis of the axle system is performed with the axle system used for the test vehicle, as shown in Figure 9.

Figure 9(a) shows the experimental modal analysis for the only axle case, and Figure 9(b) shows the experimental modal analysis for the assembled axle system, which is the axle system. The results for the axle case are used later for confirmation of the FE model. For the experimental modal test, 48 nodes were used for the geometry of the axle system. Figure 10 shows the sum of the frequency response function measured at 48 nodes of the axle system. The first resonance of the axle structure occurred at 77 Hz and is the first bending mode of the axle structure. Other resonance of the axle system occurred at many other frequencies.

The resonance of the axle system is correlated with the interior noise of the 9th order component occurred at 595 Hz, and is the 3rd order bending mode of the axle system. The mode shape of this 3rd bending mode is shown in Figure 11. The whine noise occurred around 550~600

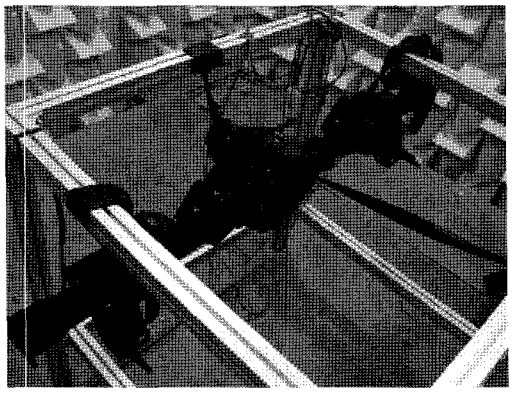

(a)

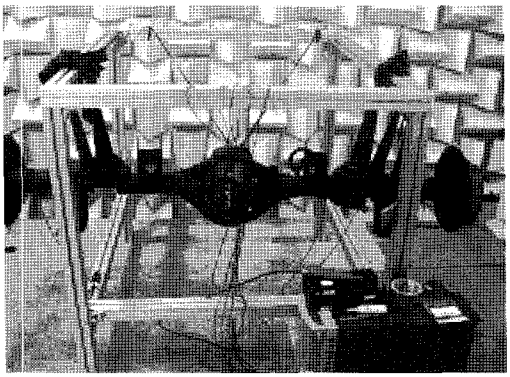

(b)

Figure 9. Photo illustrations for the experimental modal analysis (a) axle case (b) assembled axle system.

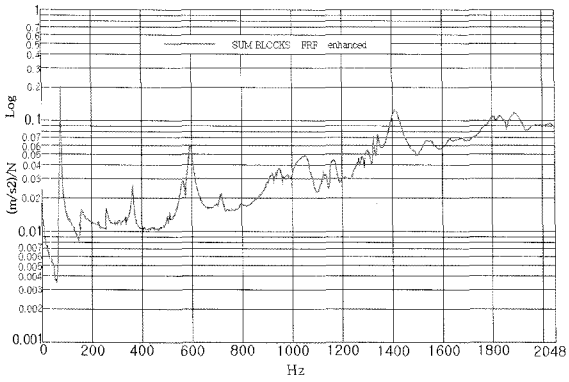

Figure 10. Sum of the frequency response function measured on the axle system for experimental modal analysis.

Hz, as shown in Figure 1. This frequency is associated with the resonance frequency of the 3rd mode.

According to the mode shape, there is serious distortion in the axle carrier cover with torsion of the axle system. In order to understand the correlation between this mode shape and the operational defection shape of the axle system, the operation deflection shape is obtain-

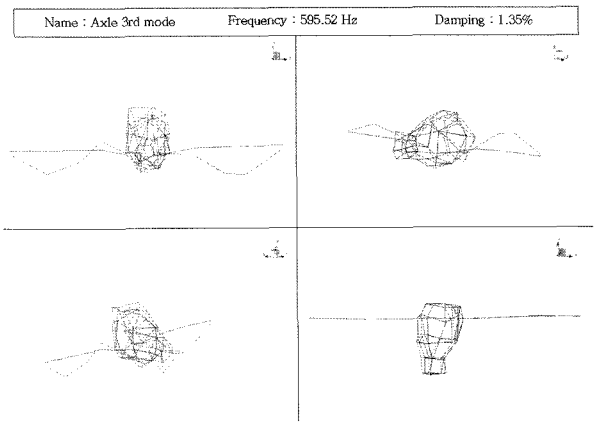

Figure 11. The 3rd mode shape of the axle system.

ed by analyzing the vibration data measured at the axle system during acceleration of the test vehicle from 1800 rpm to 4400 rpm. The ODS of the axle system is obtained by calculating the relative phase difference between the node point and the reference point. The mathematical equation is expressed as follows:

$$\phi_i = Y_i \cdot \frac{X^*}{|X|} = B \cdot e^{j(b-a)} \tag{1}$$

$$X = A \cdot e^{ja} \tag{2}$$

$$Y = B \cdot e^{ja} \tag{3}$$

where X is the spectrum of the vibration data measured at a reference point and Y_i is the spectrum of the vibration data measured at an arbitrary node point of the axle system.

Figure 12 shows the sum of the 9th order component's frequency obtained from spectrum analysis at each rpm for vibration data measured at the 39 node points. According to these results, there are three peaks around 2900 rpm (430 Hz), 3700 rpm (555 Hz) and 4000 rpm (600 Hz). Among the three peaks, the two peaks above 3600 rpm are related to the interior noise due to the

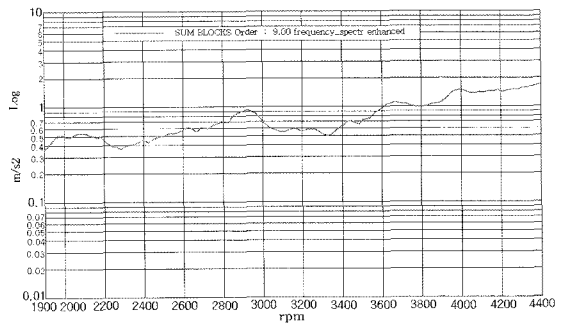

Figure 12. Sum of the frequency spectra for the 9th order component from vibration data measured at 39 node points of the axle system during acceleration.

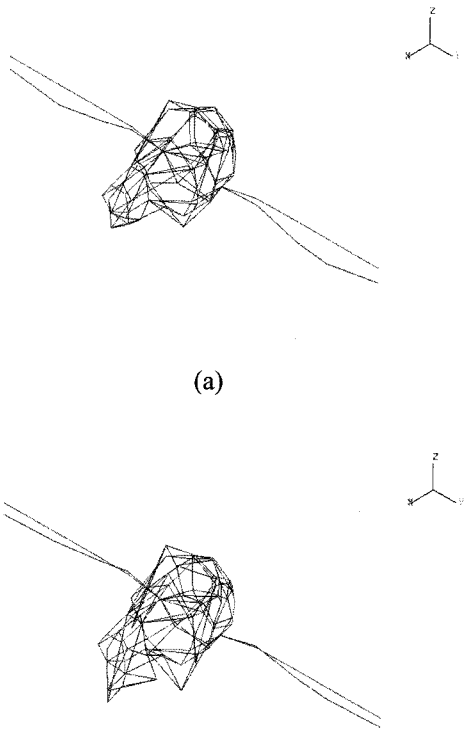

(a)

(b)

Figure 13. Operational deflection shapes at 3400 rpm and 4200 rpm (a) 3700 rpm (550 Hz) (b) 4000 rpm (600 Hz).

vibration of the axle system as shown in Figure 2. Figure 13(a) shows the ODS of the axle system at 3700 rpm, and Figure 13(b) shows the ODS of the axle system at 4000 rpm. The operational deflection shape at these two speeds is similar to the mode shape of the axle system with a natural frequency of around 595 Hz from the frequency response functions shown in Figure 11. The major operational deflection shape at this frequency is the distortion of axle carrier cover with the torsion of the axle system. The contact force cause by meshing between the ring gear and pinion gear excites the structure of the axle carrier and carrier cover and causes them to vibrate. This vibration of the axle structures disturbs the air around them and radiates the noise which is then transferred directly inside of the car through the car body.

4. FINITE ELEMENT ANALYSIS FOR THE AXLE SYSTEM

4.1. FE Model for the Axle System and Its Modal Analysis

Figure 14 shows the FE model of the axle system. The

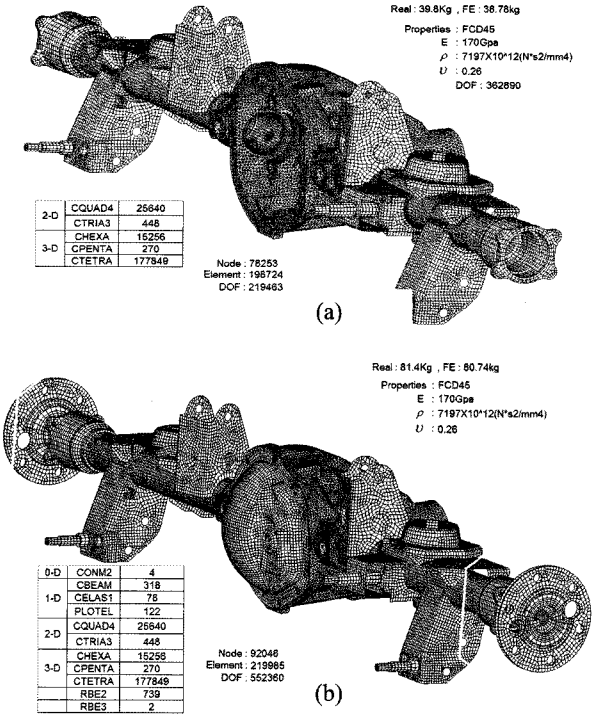

Figure 14. Finite element model of the axle system (a) axle case model (b) assembled axle model.

axle system is composed of the axle carrier, shaft housing, shaft bracket, carrier cover and difference gear inside of the axle carrier. For the FE model of all of the components, one-dimensional, two-dimensional and three-dimensional finite element models are used; the difference gear is modeled by using a concentrated mass with mass and inertia moment. The welding point between a component and bracket is connected with the connection method. All bearing parts are connected with the spring model. Finally, this FE model is confirmed with the results of experiment modal analysis. An analytic modal analysis using the FE model of the axle system is performed with MSC/NASTRAN. Throughout the analytical modal analysis with the FE model, the mode shape, natural frequency and modal vector are calculated. These results are compared with those of experimental modal analysis for confirmation of the accuracy of the FE model. For correct modal analysis, at the first step, analytical modal analysis for components of the axle system is performed and its results are compared with the results of experimental modal analysis. For this validation, MAC (Modal Assurance Criterion) analysis is generally used. As the MAC analysis is one method of evaluating the orthogonal property for natural vectors of the vibration system, if the two natural vectors are the same directional vector, the MAC value becomes one. If two natural vectors have orthogonal property, the MAC value is zero.

Table 1. Comparison of natural frequencies for the axle-case model.

	FEM	TEST	Error (%)	MAC
1	144.7	146.19	−1.02	0.99
2	289.2	286.38	0.9	0.99
3	517.1	527.00	−1.9	0.97
4	554.6	551.00	0.6	0.94
5	605.5	600.00	0.83	0.98
6	702.1	702.76	−0.1	0.96

Table 2. Comparison of natural frequency for the assembled axle system model.

	FEM	TEST	Error (%)	MAC
1	85	77.8	8.2	0.97
2	155.5	155.1	0.25	0.87
3	332	361.8	−8.7	0.75
4	558.5	595.5	−6	0.93

The mathematical expression is given by,

$$MAC_{ij}=\frac{\left|\{\Phi_{TEST}\}_i^T\{\Phi_{FEM}\}_j\right|^2}{[\{\Phi_{TEST}\}_i^T\{\Phi^*_{TEST}\}_j\{\Phi_{FEM}\}_i^T\{\Phi^*_{FEM}\}_j]} \quad (4)$$

where Φ is the nature vector for the natural mode shape at each natural frequency of the vibration system. Figure 14(a) shows the FE model of the axle case. The modal analysis results obtained by using FEM and EMA for the axle case are listed in Table 1 for a comparison of the two results. According to these results, the MAC values for each mode are over 0.94 and errors are under 2%. Therefore, the FE model of the axle case is sufficient for the vibration analysis. Figure 15 shows the mode shapes of the axle case for the natural frequencies obtained by using FEM and EMA. As the next step, the shaft and difference gear were assembled with the axle case as shown in Figure 14(b). The modal analysis results obtained by using FEM and EMA for the assembled axle system are listed in Table 2.

According to these results, MAC values for each mode are over 0.7 and errors are under 10%. Even if these results have few high errors and small MAC values compared with the results for the axle case, these results are still useful for the optimization of the axle system by using FEM. Figure 16 shows the mode shapes of the assembled axle system for the natural frequencies obtained by using FEM and EMA. Figure 17(a) shows the sum of the frequency response function for the axle case and Figure 17(b) shows the sum of the frequency response function for the assembled axle system. The dotted line is

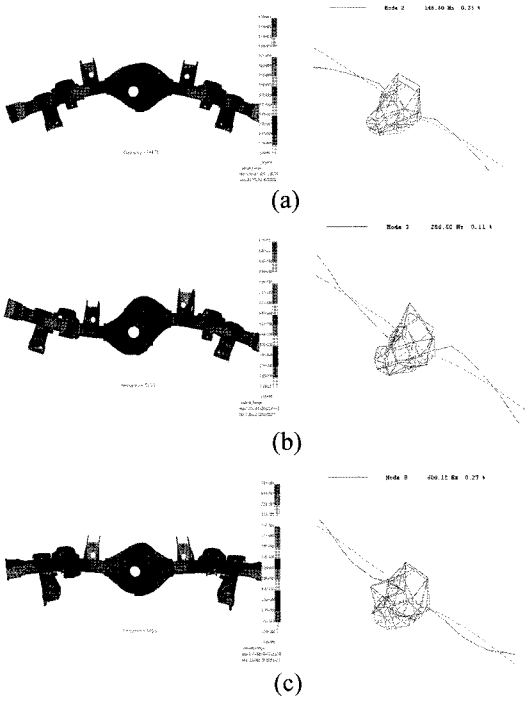

Figure 15. Comparison between mode shapes of axle case by the analytical method and that by the experimental method (a) 144.7 Hz (b) 289 Hz (c) 605.5 Hz.

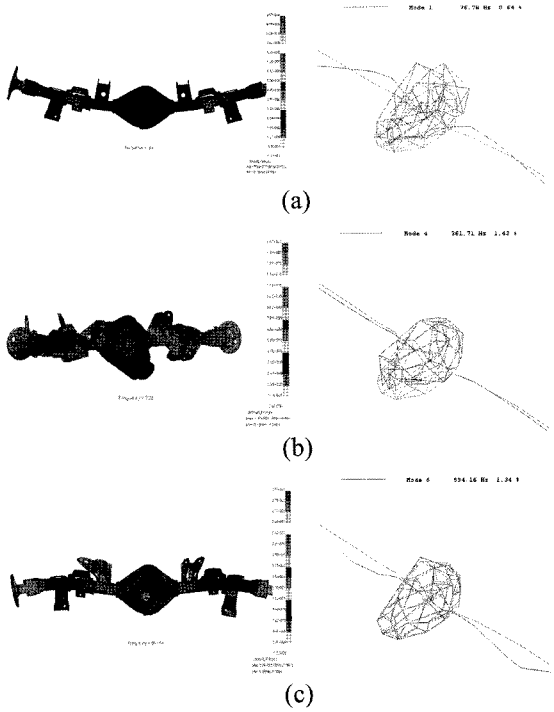

Figure 16. Comparison between mode shapes of assembled axle model by the analytical method and that by the experimental method (a) 144.7 Hz (b) 289 Hz (c) 605.5 Hz.

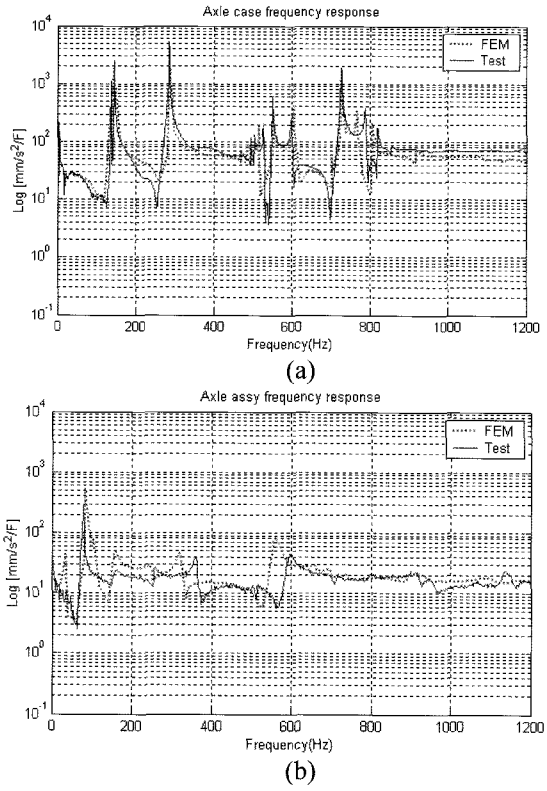

Figure 17. Comparison of the frequency response function for FEM and EMA (a) axle case (b) assembled axle system.

related to the FEM and the solid line is related to the EMA. A resonance frequency around 595 Hz is important because the mode shape at the frequency is correlated with the interior noise. According to Table 2, at this frequency, the error is 6% and the MAC value is 0.93. Therefore, this FE model is reasonable for vibration analysis because the error is within 10%. This axle system assembly is used for the optimization of the axle system with a low noise level

4.2. Estimation of Bearing Force

For the forced vibration analysis of the axle system, the force exciting the axle system at the bearing should be estimated. This force is obtained by the inverse force identification method using singular value decomposition (Warwick *et al.*, 1993). The inverse force identification method is based on the frequency response between the vibration-measuring point on the axle system and the exciting point at the bearing. The vibration-measuring point on the axle system is the 39 points used for the ODS. The exciting point is four points. Two points exciting the axle system are the bearings located at both ends of the flange. The other two exciting points are the bearings located at both ends of axle shaft housing. The

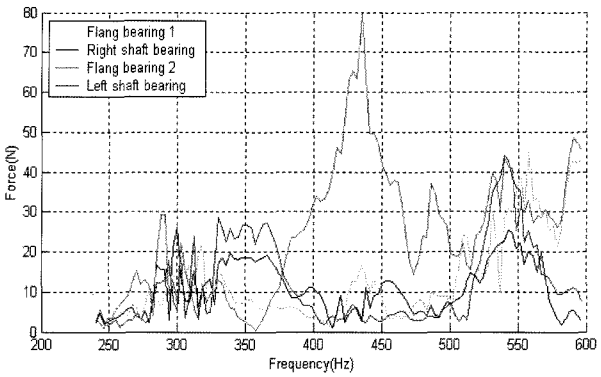

Figure 18. Estimation of bearing force of the axle system.

mathematical equation used for the estimation of the bearing force is expressed as follows:

$$\{\mathbf{f}\}=[\mathbf{H}]^{-1}\{\mathbf{a}\} \quad (5)$$

where vector $\{\mathbf{a}\}$ is the acceleration vector for the vibration-measuring point, vector $\{\mathbf{f}\}$ is the force vector being estimated, and matrix vector $[\mathbf{H}]$ is the matrix with a frequency transfer function between the vibration-measuring point and excitation point. This transfer matrix is not a rectangular matrix since the number of elements in the force vector is different from the number of elements in the acceleration vector. Therefore, the force vector is calculated by using singular value decomposition. Figure 18 shows the force spectrum calculated by the inverse force identification method. This estimated force is used for the forced vibration to predict the radiated noise from the axle system.

5. MODIFICATION OF THE STRUCTURE OF THE AXLE SYSTEM

5.1. Forced Vibration of the Axle System

For forced vibration analysis, the forces estimated in the previous section were used and the axle system is constrained with boundary conditions corresponding to the condition of the test vehicle. Figure 19 shows the analytical ODS of the axle system at 550 Hz and at 600 Hz with the constrained boundary condition of the assembled axle system. This analytical ODS of the assembled axle system is similar to the ODS obtained by measurement, as shown in Figure 13.

The ODS of the assembled axle system is the distortion of the axle carrier cover with the torsion of the axle system. Therefore, in order to reduce the vibration, the axle cover is reinforced not only by stiffening the axle cover with a rib as shown in Figure 20, but also by increasing the thickness of the carrier from 1.8mm to 3.3 mm. This modification method is to reduce the surface vibration of the axle cover and, finally, the noise radiated

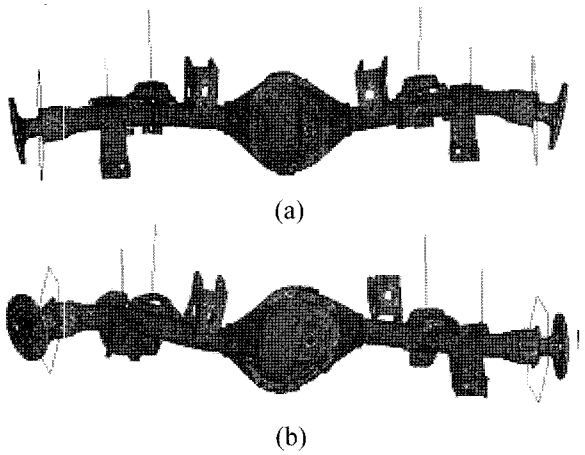

(a)

(b)

Figure 19. Operational deflection shapes at 550 Hz and 600 Hz.

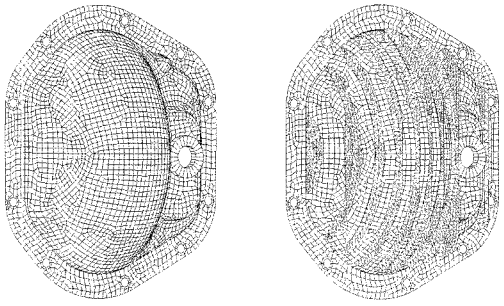

Figure 20. Modification of the axle cover for the noise reduction (a) original (b) modified.

from the axle system.

5.2. Prediction of the Noise by the BEM Model

The BEM model of the axle system is required to predict the noise radiated by the vibration of the axle system. In this study, for noise prediction, the BEM indirect method of "Virtual Lab" made by LMS Co. was used. The structural mesh of the FE model generates the acoustic mesh for BEM. The acoustic mesh is used to predict the sound pressure level at the acoustic field point. Figure 21 shows the acoustic mesh of the axle system for the sound prediction by using BEM.

This acoustic mesh is made by 4-node shell elements. The length between each node is less than 180 mm. With this element, the maximum frequency range for the noise analysis is 1800 Hz. The acoustic field point is selected according to the regulation ISO-3744, as shown in Figure 22. The acoustic field radius is 1670 mm from the center of the axle system to the top or to the bottom and 1942 mm to the front or rear. The target direction for noise reduction among acoustic field points is the front-top direction in the acoustic field. This direction is the nearest to the car body. Figure 23 shows the predicted sound

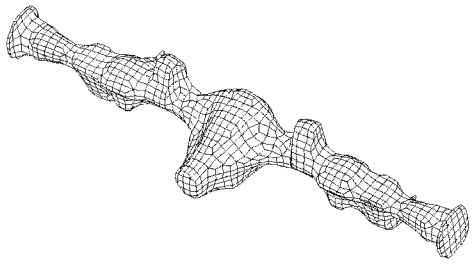

Figure 21. Acoustic mesh for the sound prediction by using BEM.

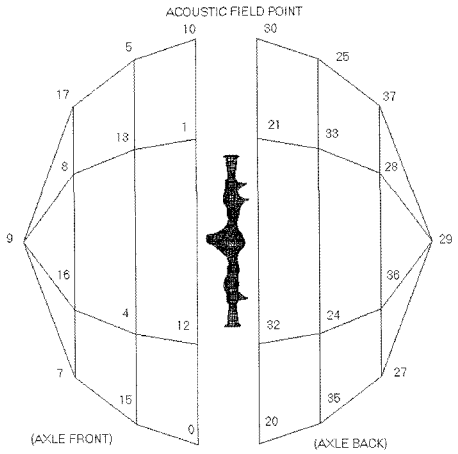

Figure 22. Acoustic field point for the noise analysis for the axle system by using BEM.

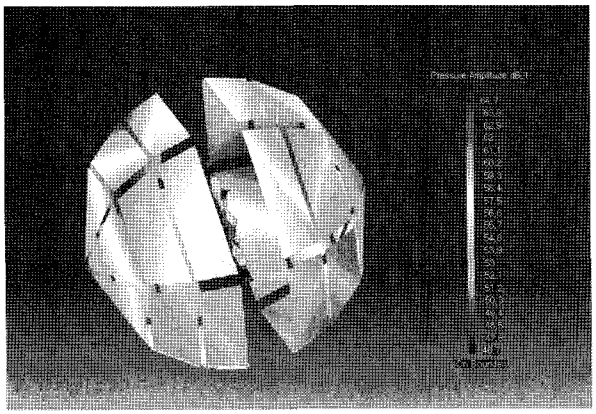

Figure 23. Result of the noise analysis for the axle system by using BEM.

pressure level at the acoustic field points. These results are obtained by using BEM. Figure 24 shows the sound pressure level of the axle system estimated by the FE model and BEM at arbitrary points of the front-top direction in the acoustic field. In Figure 24, the solid line means the sound pressure level for the original axle system. The dotted line means the sound pressure level

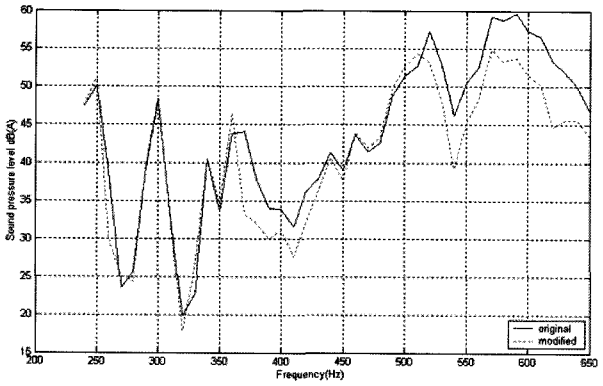

Figure 24. Sound pressure level of the axle system estimated by the FE model and BEM.

for the modified axle system. The sound pressure level at the frequency band between 500 and 630 Hz is reduced by 3dBA after modification. We tried to modify other components such as the shaft housing and carrier structure, but this modification was not effective for the noise reduction of the axle system.

6. CONCLUSIONS

Throughout the baseline noise test of the test vehicle, the whine noise of the 9th order component of the speed of the propeller shaft was over 50dBA at 3600~4400 rpm, which is the target sound pressure level for recognition of the whine noise level. In order to reduce this whine noise, the noise source was identified by using the EMA and ODS. It is inferred that the whine noise source is airborne noise due to the vibration of the axle system but not structure-borne noise, since the isolation rubber and mounting rubber reduced the vibration transmitted from the axle system to the body throughout the 5-link suspension and the chassis frame. Therefore, the major source of the 9th order interior noise component is associated with the airborne-noise radiated by the axle system. Throughout the EMA and ODS analyses, it was found that the 3rd order mode shape of the axle system at 590 Hz is associated with the 9th order interior noise component. Its mode shape is the distortion of the axle carrier cover with the torsion of the axle system. The axle system is modeled by the FE model, which was used for the BEM analysis to predict the sound pressure level. The accuracy of the FE model is confirmed with the EMA. The bearing force of the axle system was estimated by using the inverse force estimation method based on the singular value method. This estimated force was used for the analysis of the forced vibration of the FE model of the axle system. The forced vibration and the boundary element model were used for the noise prediction of the axle system. In order to reduce the vibration and radiation noise of the axle system, the stiffness of the axle system was changed by stiffening the rib on the carrier cover and increasing the thickness of the carrier. The predicted noise of the axle system was reduced by 3~4dBA according to the results of the simulation by using the BEM model.

ACKNOWLEDGEMENT–This work was supported by INHA UNIVERSITY Research Grant.

REFERENCES

Becker, S. B. and Yu, S. (1999a). Gear noise rating prediction based on objective measurement. *SAE Paper No.* 1999-01-1721.

Becker, S. B. and Yu, S. (1999b). Objective noise rating of gear whine. *SAE Paper No.* 1999-01-1720.

Blakely, K. (1999). Updating Msc/ Nastran nodels to match test data. *Proc. MSC World Users Conf.* 1–30.

Donley, M. G., Lim T. C. and Steyer, G. C. (1992). Dynamic analysis of automotive gearing systems. *J. Passenger Cars: Mechanical Systems* **101, 6,** 958–968.

Kim, S. J. and Lee, S. K. (2007). Experimental Identification on a gear whine noise in the axle system of a passenger van. *Int. J. Automotive Techenology* **8, 1,** 75–82.

Lee, S. K., Kim, B. S. and Park, D. C. (2005). Objective evaluation of the rumbling sound in passenger cars based on an artificial neural network. *J. Automobile Engineering* **219**, **4**, 457–469.

Lee, S. K. and Chae, H. C. (2004). The application of artificial neural networks to the characterization of interior noise booming in passenger cars. *J. Automobile Engineering* **218**, **1**, 33–42.

Paras, M. M. (2003). Validation of a system of finite element models representing a complex transaxle. *SAE Paper No.* 2003-01-1594.

Sun, Z., Steyer, G. Meinhardt, G. and Ranek R. (2003). NVH robustness design of axle system. *SAE Paper No.* 2003-01-1492.

Walter, O. and Kaiser, H. J. (1990). Finite element analysis of dynamic behavior of an engine block and comparison with experimental modal test results. *Proc. MSC World Users Conf.* 10–20.

Warwick, D. C. and Gilheany, J. J. (1993). Dynamic force estimation via modal decomposition of operational response measurements in a multi source environmental. *11th IMAC.* 1–15.

Wyckaert, K. and Van der Auweraer, H. (1995). Operational analysis, transfer path analysis, modal analysis. Tools to understand road noise problem in car. *SAE Paper No.* 951751.

Zwicker, E. and Fastl, H. (1999). *Psychoacoustics: Facts and Models.* 2nd Edn.. Springer-Verlag. Berlin.